JOURNAL OF MATERIALS SCIENCE 25 (1990) 3215–3220

Piezoelectricity and microstructures of modified lead titanate ceramics

D. R. DE VILLIERS, H. K. SCHMID
Division of Materials Science and Technology, CSIR PO Box 395, Pretoria 0001, South Africa

Modified lead titanate ceramics with the composition $Pb_{0.70}$ $Ca_{0.30}$ $Ti_{0.94}$ $(Co_{1/2}W_{1/2})_{0.06}$ O_3 with 1 mol% MnO were prepared by the mixed oxide route. By varying the sintering temperature, ceramics with average grain sizes between 2.8 and 5 μm were obtained. An increase in grain size resulted in an increased electromechanical anisotropy and a decreased dielectric constant. Transmission electron microscopy was used to examine the ferroelectric domain boundaries and intergranular phases. Indications are that during poling favourably oriented domains approximately doubled in size by 90° type domain wall switching. Evidence was found for the existence of a vitreous intergranular phase at multiple grain junctions. EDS microanalysis indicated that the amorphous grain boundary phase had a lower lead content than the bulk material.

1. Introduction

Lead titanate is a well-known perovskite-type ferroelectric material with good piezoelectric properties. At temperatures below the Curie point $T_c = 490°C$ its crystal structure has tetragonal symmetry with a c/a ratio of about 1.063. Pure $PbTiO_3$ ceramics obtained by the usual powder processing method disintegrate during cooling and have no practical application as a ferroelectric material. The mechanical weakness is caused by internal stress brought about during cooling due to the cubic to tetragonal transition and also its rather large anisotropic thermal expansion [1]. It is now well established that a large number of elements might be suitable additives for partial substitution of A and B site cations in order to reduce spontaneous strain and inhibit cracking [2–4]. Recently chemically modified lead titanate ceramics (MPT) have aroused interest due to their highly anisotropic piezoelectric coupling factors. Yamashita *et al.* [5] produced $Pb_{1-x}Ca_xTi_{0.96}$ $(Co_{1/2}W_{1/2})_{0.04}O_3$ ceramics (with $x = 0.12$ and 0.24) which had low porosities and showed highly anisotropic electromechanical properties. For this type of MPT ceramic the piezoelectric constant, d_{33}, could be increased by increasing the fraction of the Ca^{2+}, Co^{2+} and W^{6+} modifiers as was reported by Takeuchi *et al.* [6]. The increase in modifiers also resulted in an increased dielectric constant and a reduced tetragonality. The latter effect is in accordance with earlier reports that the c/a ratio decreases with increasing substitution of calcium for lead [7].

The highly anisotropic electromechanical properties make these ceramics very promising for special piezoelectric applications such as ultrasonic imaging devices and underwater hydrophones. The mechanical and piezoelectric properties are influenced by the amounts of additives in the composition and by the processing conditions. Unfortunately, limitations often occur due to the presence of residual intergranular phases that result from liquid phase sintering. Such second phases are normally in a vitreous state and form in most cases either from sintering aids or from impurities present in the starting materials. Intergranular phases normally assist densification during sintering and influence grain growth, however, their presence may have detrimental effects on the mechanical and electrical properties of the ceramics. Hence a detailed understanding of the microstructure of the interfaces and the morphology and composition of intergranular phases is of fundamental importance in order to optimize the properties of these materials.

The purpose of this study was to investigate some of the properties and microstructure of a Ca–Co–W modified lead titanate. Emphasis was also placed on the microstructural characterization of the interfaces by means of transmission electron microscopy (TEM) and the microanalysis of residual intergranular phases by means of energy-dispersive X-ray spectroscopy (EDS).

2. Experimental procedure

A MPT ceramic with nominal composition $Pb_{0.70}$ $Ca_{0.30}Ti_{0.94}$ $(Co_{1/2}W_{1/2})_{0.06}O_3$ plus 1 mol% MnO was prepared from chemically pure PbO, $CaCO_3$, TiO_2, Co_3O_4, WO_3 and $MnCO_3$. 1 mol% PbO was added in excess of the nominal composition in order to compensate for lead evaporation during processing. The raw materials were ball milled for 24 h in distilled water with zirconia milling media. After drying the powder it was calcined in a covered alumina crucible at 1000° C for 2 h. The calcined lumps were crushed in a mortar and attrition milled for 4 h with zirconia milling media to reduce the mean particle size to about 0.5 μm. After drying a PVA binder solution was added to the mixture. Disc and bar shaped green compacts were produced by uniaxially cold pressing the powder at 80 MPa. The green compacts were sintered in a covered alumina crucible for 5 h at a temperature of

0022–2461/90 $03.00 + .12

either 1040, 1080 or 1120° C. The sintered discs were about 10.5 mm in diameter and were ground to a thickness of about 0.8 mm; the bars were ground to dimensions of about 2.5 × 5 × 25 mm. After grinding, silver electrodes were fired onto the major faces for the electrical measurements. The material was poled by placing the samples in an oil bath at 110° C and applying an electric field of 50 kV cm^{-1} for 5 min.

Lattice parameters were measured by X-ray powder diffraction (XRD) using silicon as a standard. For the poled material the c/a ratios were approximated from the relative positions of the (2 0 0) and (0 0 2) X-ray reflections obtained from compact ceramic samples after dissolving off the silver electrodes in concentrated nitric acid.

Measurements were made at room temperature allowing at least 24 h after poling for ageing of properties. Piezoelectric properties and coupling factors were determined by the resonance method using frequency data from an impedance analyser (HP 4192 A). The thickness coupling factor k_t was calculated from the ratio of the overtone frequency to the fundamental frequency of the thickness mode series resonance using Onoe's table [8]. The piezoelectric constant d_{33} was measured at 100 Hz by a Berlincourt Piezo d_{33} meter.

A poled ceramic sintered at 1120° C was used for transmission electron microscopy studies. Thin electron transparent foils were obtained by cutting the sintered sample with a diamond saw into slices 120 μm thick and ultrasonically drilling 3 mm discs. The discs were further thinned by mechanical dimple grinding and polishing down to a thickness $t \approx 10\,\mu$m at the centre of the discs followed by ion-milling (5 kV Ar ions, 12° angle of incidence). The samples were examined in an analytical scanning transmission electron microscope* (STEM), operated at an accelerating voltage of 120 kV. The instrument was equipped with an energy-dispersive X-ray spectrometer* (EDS) attachment for chemical microanalysis with high spatial resolution.

3. Results and discussion

3.1. Electrical properties

The weight losses, mainly due to PbO evaporation during sintering, varied from about 0.6 wt % for sintering at 1040° C to about 0.8 wt % for sintering at 1120° C resulting in very similar compositions for all sintered samples. The densities of individual sintered ceramics were between 97.5 and 99% of theoretical density. Both the mean grain size of the ceramics and the electromechanical anisotropy k_t/k_p increased with an increase in sintering temperature (Fig. 1). The ratio k_t/k_p of the planar and thickness coupling factors increased from about 9 to 12. This is due to a drop in k_p while k_t remains almost constant. As the grain size increased the dielectric constant decreased while the dielectric losses appeared to be independent of grain size. A similar relationship between grain size, electromechanical anisotropy and dielectric constant was reported by Takeuchi *et al.* [6]. They found that

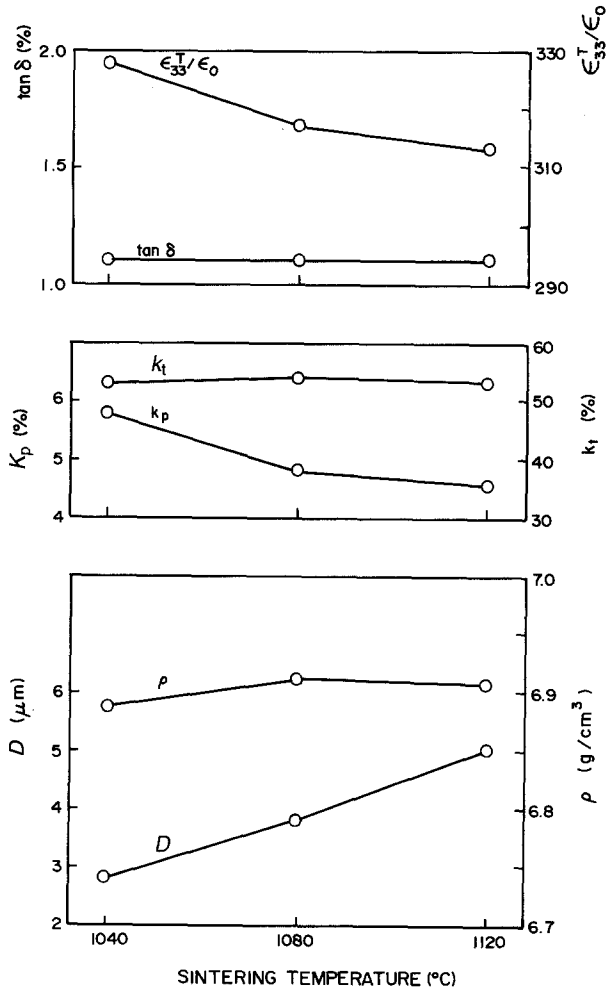

Figure 1 Dielectric constant, $\varepsilon_{33}^T/\varepsilon_0$; dielectric loss, tan δ; electromechanical coupling factors k_t and k_p; density ρ and mean grain size D as a function of sintering temperature.

an increase in sintering time resulted in a larger grain size, an increase in electromechanical anisotropy and a decrease in the dielectric constant in $(Pb_{1-x}Ca_x)Ti_{0.94}(Co_{1/2}W_{1/2})_{0.06}O_3$ MPT ceramics where $0.34 \leqslant x \leqslant 0.38$. Powder X-ray diffraction data indicated a tetragonality of $c/a = 1.025$ for all three samples irrespective of sinter temperatures. The c/a ratios determined from the surfaces of bulk samples after poling also remained constant at 1.025 independent of

TABLE I Properties of $Pb_{0.70}Ca_{0.30}Ti_{0.94}(Co_{1/2}W_{1/2})_{0.06}O_3$ with 1 mol % MnO

Density	(g cm^{-3})	6.91
Lattice parameters	a (nm)	0.3900
	c (nm)	0.3999
Dielectric constant	$\varepsilon_{33}^T/\varepsilon_0$ (at 1 kHz)	313
Dielectric loss	tan δ (at 1 kHz) (%)	1.1
Planar coupling factor	k_p	0.045
Thickness coupling factor	k_t	0.53
Piezoelectric constant	d_{31} (10^{-12} C N^{-1})	−4.6
	d_{33} (10^{-12} C N^{-1})	85
Hydrostatic coefficient	$d_h g_h$ (10^{-15} m^2 N^{-1})	2070
Frequency constant	N_p (Hz, m)	2950
	N_t (Hz, m)	2190

*Philips EM 420 analytical STEM with EDAX PV 9900 EDS and GATAN 607 EELS attachments

sinter temperature. Jyomura *et al.* [9] observed a slight increase in c/a ratios when the grain size of (Pb Nd) (TiMnIn)O_3 ceramics was increased from 0.7 to 10 μm. The increase in tetragonality is thought to result from reduced stresses in larger grained ceramics. This effect may have been too small to be noticeable in the present study where a relatively small increase in the mean grain size from 2.8 to 5 μm was observed. Some properties of the MPT ceramic sintered at 1120° C, which showed the highest electromechanical anisotropy, are listed in Table I. This material has a favourable hydrostatic coefficient $d_h g_h$ $(=(d_{33} + 2d_{31})(g_{33} + 2g_{31}))$ for a MPT ceramic due to its relatively large d_{33} and high anisotropy. It is known that poling conditions also influence the k_p. An increase in poling field was shown to lower the k_p for a calcium MPT ceramic [10]. The grain size therefore appears to have an effect upon the domain orientation which influences the k_p. The relationship between the larger electromechanical ansiotropy of $PbTiO_3$ ceramics and the small anisotropy of its single crystals (or domains) has been demonstrated by Turik *et al.* [11].

3.2. Microstructure

3.2.1. Ferroelectric domain boundaries

Typical ferroelectric domain structures, as observed in the poled MPT ceramics, are depicted in Fig. 2. The TEM bright-field (BF) micrograph in Fig. 2a shows 90°-type ferroelectric domain boundaries oriented parallel to $(\bar{1}\,1\,0)$ crystallographic planes. These domain walls are $\{1\,1\,0\}$ transformation twins; their 90° nature can be verified by electron diffraction techniques. As the cubic (paraelectric) phase is cooled through the Curie point, the unit cell deforms towards tetragonal symmetry (ferroelectric phase) and transformation strain will be reduced by twinning on planes of minimum average distortion (martensitic transformation). In order to cancel the transformation strains exactly, four equal shears of magnitude $\varepsilon/2$ are required in this twin system [12]. In the case of 90° walls this small angle of distortion, which depends on the c/a ratio of the tetragonal phase, gives rise to diffraction spot splitting across $(1\,1\,0)$ as shown in the inset in Fig. 2a. The splitting angle 2ϕ defines the deviation from normality of the c-axes of adjacent twin variants and is related to the c/a ratio of the tetragonal phase by

$$\tan(\pi/4 + \phi) = c/a.$$

In the case of 180° walls, where the polarization vectors (c-axes) of adjacent domains are in antiparallel orientation, all diffraction spots are expected to coincide and no splitting would be observed. The measured angle $2\phi \approx 1.6\ (\pm\ 0.5)$ degree corresponds to a tetragonality $c/a \approx 1.028\ (\pm\ 0.009)$ which is in good agreement with X-ray diffraction data (Table I).

By applying the theory of martensitic transformation [13] the fractions X and $(1-X)$ of the twin variants can be calculated as a function of the lattice parameters of the cubic and tetragonal phases. In the present case the ratio $c/a = 1.025$ yields a theoretical equilibrium domain width ratio $X/(1-X) = 2/1$, whereas in the poled material the observed domain width ratio varied between 3.5 and 5.3. The experi-

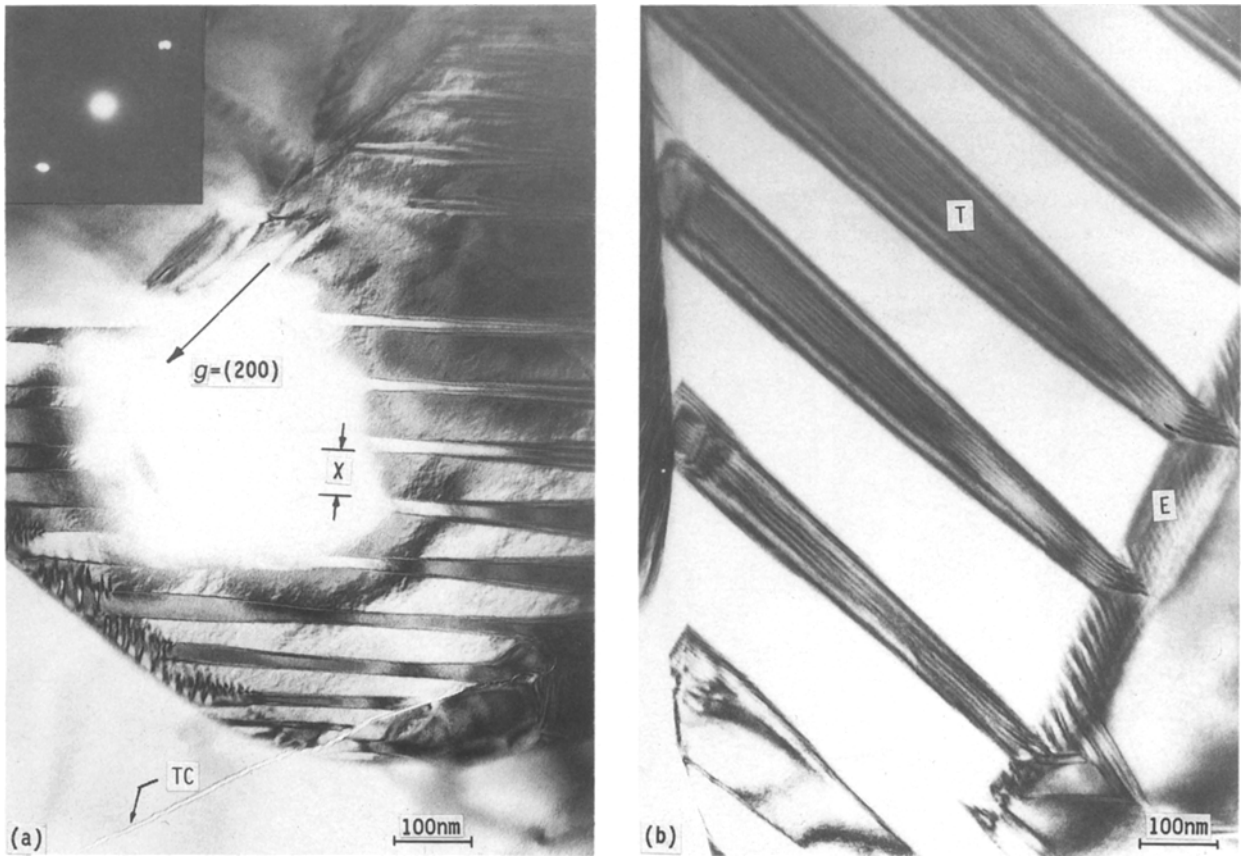

Figure 2 TEM BF micrograph showing ferroelectric domain boundaries. (a) 90° twin related domain walls close to edge-on orientation, (TC transgranular crack); (b) boundaries tilted, (T twin related 90° walls, E substructurally twinned end walls).

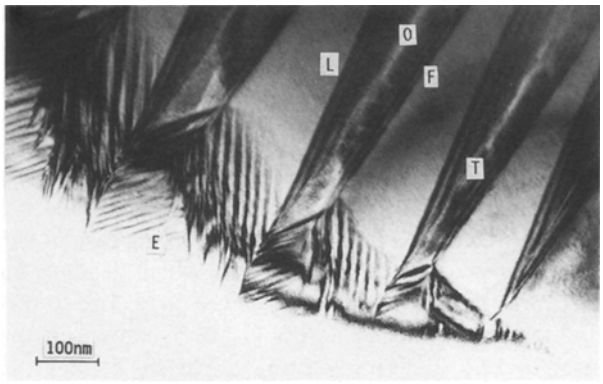

Figure 3 Ferroelectric domain boundaries on ($\bar{1}$ 1 0) plane (tilted). (T 90° walls; E, end walls showing substructural twinning; F, first fringe at top (entrance) surface, O; overlap region; L, last fringe at bottom (exit) surface).

mental ratios suggest that during the poling process the size of the favourably oriented twin variant (in respect to the external poling field) doubled in size at the expense of the other twin variant. This is consistent with our observations that in the poled material 90° walls occur as relatively narrow-spaced pairs of twin-related domain boundaries (lateral spacing $d \approx$ 20 nm). The growth of favourably oriented domains by 90° switching is evidenced by an increase in the I_{001}/I_{100} ratio after poling, where I_{001} and I_{100} are the intensities of the (0 0 1) and (1 0 0) X-ray diffraction peaks, respectively. The slight deviation from normality of adjacent twin variants gives rise to a distinct areal contrast between adjacent domains imaged under dynamical conditions (Fig. 2a) due to a small change in the excitation error s across coherent interfaces and results in characteristic δ-type fringe contrasts in tilted domain boundaries [14]. However, due to the narrow lateral spacing of pairs of domain walls the contrasts of tilted boundaries will overlap in thicker sample areas giving rise to a pseudosymmetrical fringe pattern under BF imaging conditions (Figs 2b and 3). These pairs of 90° domain boundaries often terminate at zig-zag shaped domain walls showing a herringbone-like substructural twin pattern (Fig. 3), similar to reports on domain structures in PZT ceramics [15]. The lateral spacings of substructural twins, which seem to be oriented also on {1 1 0} planes, are in the order of 15 to 20 nm. It is assumed that this substructural twinning phenomenon arises in regions of high strain in accordance with similar observations in PZT ceramics [16].

3.2.2. Grain boundaries

The microstructure of grain boundaries was studied by means of conventional TEM at high magnification. Fig. 4 shows a series of TEM bright-field (BF) micrographs of a typical triple grain junction (TJ) as observed in this material. The grain boundaries (labelled GBI, II and III) are imaged in edge-on orientation. The presence of a residual intergranular phase situated in a small pocket at the TJ is clearly distinguishable from the crystalline MPT matrix phase. Microdiffraction experiments as well as the lack of diffraction contrast in tilting experiments indicated a vitreous state for this second grain boundary phase. In the case of small pockets (diameter $d \leqslant$ 10 nm) the solid–liquid (SL) interphase interfaces between the crystalline matrix and the amorphous intergranular phase were smoothly curved at the corners of grains resulting in small dihedral angles of SL interfaces at grain boundaries. The curved interfaces have a physical significance in that the sign of curvature as observed in this material indicates a thermodynamically stable intergranular phase which at equilibrium is penetrating along grain boundaries resulting in wetted grain surfaces. The wetting of grain boundaries by the intergranular glassy phase was

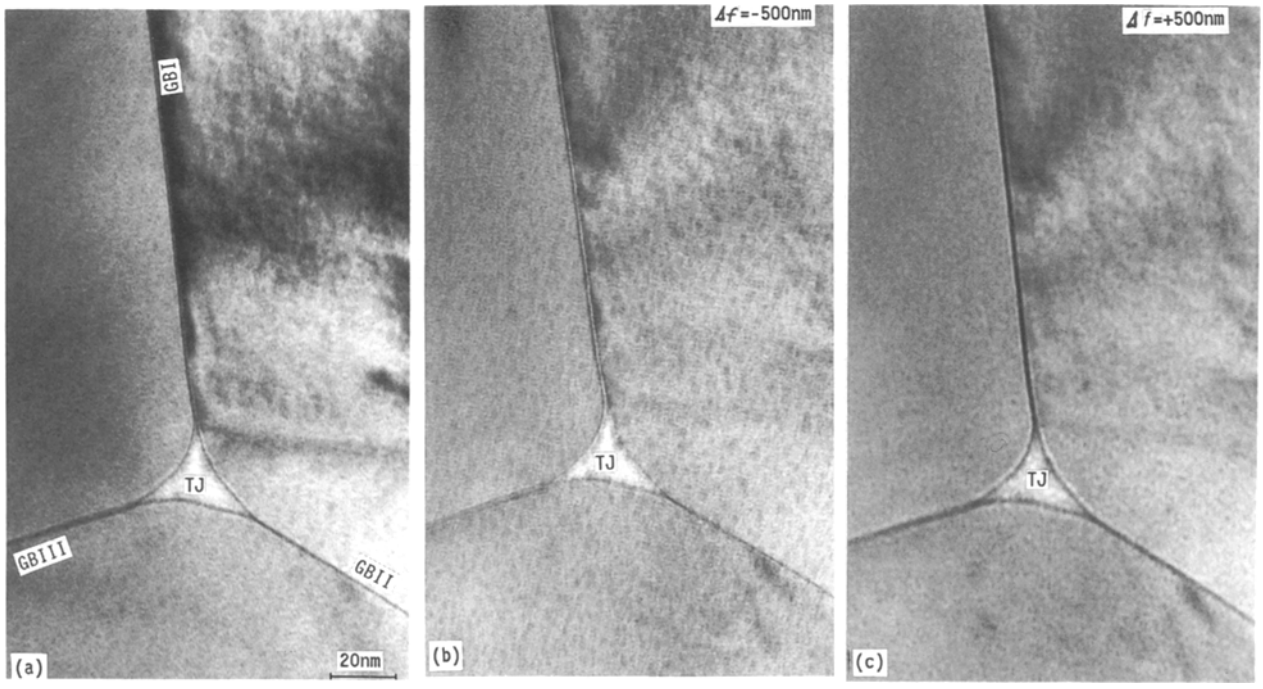

Figure 4 Intergranular phase at triple grain junction (TJ). (a) TEM BF micrograph in-focus; (b) underfocused; (c) overfocused, showing Fresnel fringe contrast at wetted grain boundaries (GB).

confirmed by out-of-focus imaging of grain boundaries in edge-on orientation. Under these imaging conditions grain boundaries wetted by a thin film of intergranular phase give rise to Fresnel diffraction patterns [17] as shown in Figs 4b and 4c. The analysis of Fresnel fringes as a function of defocus distance Δf indicated that thicknesses for the intergranular films at grain boundaries were of the order of $\delta \approx 1$ nm. Results on TEM investigations on the microstructure of grain boundaries in MPT ceramics are reported in more detail elsewhere [18]. Occasionally, cracks were observed in this MPT ceramic. The fracture surfaces indicated a preponderance of transgranular cracking (TC), as seen for example in Fig. 2a. It can be concluded that the bonding strength of wetted grain boundaries is relatively high and considering the necessary condition for wetting results in the relation $2\gamma_{SL} < \gamma_{SS}(hkl) < 2\gamma_{FS}(hkl)$ for surfacial and interfacial energies in this material, where γ_{SL} is the energy of the solid–liquid interface, $\gamma_{SS}(hkl)$ is the energy of a "clean" crystalline interface (hkl), and $\gamma_{FS}(hkl)$ is the energy of the free surface (hkl). As pointed out by Clarke [19], the most important practical implication of these observations is that if an intergranular phase wets the grain boundaries, then it will have an equilibrium thickness and cannot be removed during sintering except by altering its interfacial energy by means of altering its chemical composition.

3.3. Microanalysis

The chemical composition of the MPT matrix phase and the residual intergranular phase was analysed in thin sample sections by means of standardless quantitative EDS analysis in STEM mode. The results of the EDS analysis are summarized in Table II; the relative concentrations are listed in wt % cations normalized to 100%. In order to reduce statistical errors a multiple spectra method [20] was applied. The concentrations listed in Table II are the results of 10 to 20 individual spectra which were analysed statistically at 95% confidence. EDS results from the matrix phase (bulk grain) agreed well within experimental errors to the nominal composition and confirmed the small PbO loss during materials processing. The intergranular phase situated in pockets at triple grain junctions (TJ) and in thin films at grain boundaries (GB) was analysed with high spatial resolution using a fine probe of effective electron beam spot size $D_s \approx 3$ nm. Since beam spreading cannot be neglected in this case [21], information on the chemical composition can be obtained from sample volumes in the order of $D \geqslant 5$ nm in diameter and $t \leqslant 30$ nm in thickness. The EDS analysis indicated segregation of cobalt, manganese and calcium in GB regions; the concentrations of these segregate atoms in the intergranular phase were found to increase with increasing size of pockets. Silicon impurities, which are present in the matrix phase at a concentration level below the detection limit (< 0.1 wt %) showed a similar segregation behaviour. The analysis indicated an increase in the concentration of tungsten in the intergranular phase in very small pockets at TJ and also in the SL interface regions of larger pockets, in comparison to the concentration in the matrix phase. The observations suggest that tungsten in concentrations in excess of $\approx$ 2.3 wt % cannot be readily accommodated in the vitreous GB phase and together with calcium and cobalt forms small crystalline precipitations in the SL interface regions [18].

TABLE II EDS microanalysis (wt % cations)

	Si	Ca	Ti	Mn	Co	W	Pb
Nominal	–	5.5	21.4	0.3	0.9	2.6	69.7
Bulk grain	–	5.4	22.2	0.3	0.7	2.5	68.9
Small TJ	1.0	5.9	21.1	0.8	1.3	4.0	66.2
Large TJ	21.6	9.3	8.1	1.5	3.9	2.3	53.0
GB* phase	1.4	11.8	29.3	1.4	2.3	9.1	44.4

Since the thickness of the thin films of intergranular phase at wetted grain boundaries in the material under investigation is considerably below the present resolution limit of microanalysis, information on the chemical composition of such films is difficult to obtain. In this case the sampling volume is heterogeneous and therefore EDS analysis does not yield the true composition of the GB phase directly. However, by making assumptions on (i) the electron intensity distribution function of the probe, (ii) the geometry of the sampling volume and (iii) beam broadening within the foil, it is possible to separate the X-ray production function into its matrix component and GB phase component and thus retrieve the true composition GB* of the GB phase [21, 22]. The calculations confirmed a strong segregation of calcium, maganese, cobalt and tungsten at grain boundaries in analogy to EDS results on the intergranular phase in pockets at TJs. However, the calculations also indicated that the composition of thin GB films seems to be distinctly different from the composition of the intergranular phase situated in medium sized and large pockets in that the concentration level of silicon impurities is rather low whereas titanium seems to be enriched well above the concentration level of the matrix phase (Table II). It should be pointed out that contrary to earlier reports on lead enrichments in GB areas and in intergranular phases in PZT [23] as well as in MPT [24] no indication of any lead enrichment in GB areas or in intergranular phases was observed in this material.

4. Conclusions

Ceramics of the composition $Pb_{0.70}Ca_{0.30}Ti_{0.94}(Co_{1/2}W_{1/2})_{0.06}O_3$ plus 1 mol % MnO were sintered to densities of over 97% of the theoretical value and had average grain sizes of between 2.8 and 5 μm. An increase in grain size resulting from a higher sintering temperature decreased the planar coupling factor and the dielectric constant. Ceramics with an average grain size of about 5 μm and poled in an electric field of 50 kV cm^{-1} gave a d_{33} of 85 pCN^{-1} and a k_t/k_p ratio of about 12.

The microstructure of ferroelectric domain boundaries and grain boundaries was characterized by transmission electron microscopy. The observed 90° domain walls are {1 1 0} transformation twins. Often 90° type domain boundaries terminated in substructurally twinned end domain walls, indicating zones of high

elastic strain. The c/a ratio as calculated from diffraction spot splitting across 90° domain walls is in good agreement with X-ray diffraction data (c/a = 1.025). TEM observations suggest that during poling favourably oriented domains approximately doubled in size resulting in a shift of the domain width ratio away from the equilibrium value. It has been established that vitreous intergranular phases exit in pockets at triple grain junctions in this MPT material. The glassy phase penetrates along grain boundaries, wetting the grain surfaces with a grain boundary film about 1 nm thick. EDS results indicated a segregation of calcium, manganese, cobalt and tungsten modifiers as well as silicon impurities at grain boundary regions. Calculations indicated that the chemical composition of thin films at grain bondaries was different from the composition of the intergranular phase in pockets at triple grain junctions.

References

1. E. C. SUBBARAO, *J. Amer. Ceram. Soc.* **43** (1960) 119.
2. T. Y. TIEN and W. G. CARLSON, *ibid.* **45** (1962) 567.
3. Y. MATSUO, M. FUJIMURA and H. SASAKI, *ibid.* **48** (1965) 111.
4. I. UEDA and S. IKEGAMI, *Jpn. J. Appl. Phys.* **7** (1968) 236.
5. Y. YAMASHITA, K. YOKOYAMA, H. HONDA and T. TAKAHASHI, *ibid.* **20** (Suppl. 20-4) (1981) 183.
6. K. TAKEUCHI, D. DAMJANOVIC, T. R. GURURAJA, S. J. JANG and L. E. CROSS, in Proceedings of 1986 IEEE International Symposium on Applications of Ferroelectrics, Bethlehem, Pennsylvania, June 1986 (IEEE, New York, 1986) p. 402.
7. E. SAWAGUCHI and M. L. CHARTERS, *J. Amer. Ceram. Soc.* **42** (1959) 157.
8. M. ONOE, H. F. TIERSTEN and A. H. MEITZLER, *J. Acoust. Soc. Amer.* **35** (1963) 36.
9. S. JYOMURA, K. NAGATSUMA and T. TAKEUCHI, *J. Appl. Phys.* **52** (1981) 4472.
10. Y. YAMASHITA, S. YOSHIDA and T. TAKAHASHI, *Jpn. J. Appl. Phys.* **22** (Suppl. 22-2) (1983) 40.
11. A. V. TURIK, E. G. FESENKO, V. G. GAVRILYACHENKO and G. I. KHASABOVA, *Sov. Phys. Crystallogr.* **19** (1975) 677.
12. L. E. TANNER and M. F. ASHBY, *Phys. Status Solidi* **33** (1969) 59.
13. M. S. WECHSLER, D. S. LIEBERMAN and T. A. READ, *Trans. AIME* **197** (1953) 1503.
14. R. GEVERS, P. DELAVIGNETTE, H. BLANK, J. VAN LANDUYT and S. AMELINCKX, *Phys. Status Solidi* **4** (1964) 383, **5** (1964) 595.
15. E. K. W. GOO, R. K. MISHRA and G. THOMAS, *J. Appl. Phys.* **52** (1981) 2940.
16. B. HARDIMAN, R. ZEYFANG and C. REEVES, *ibid.* **44** (1973) 5266.
17. D. R. CLARKE, *Ultramicroscopy*, **4** (1979) 33.
18. H. K. SCHMID, Silicates Industriels , *Cer. Sci. and Techn.* **54** (1989) 175.
19. D. R. CLARKE, *J. Amer. Ceram. Soc.* **70** (1987) 15.
20. D. A. BONNELL, M. RÜHLE and T. Y. TIEN, *ibid.* **69** (1986) 623.
21. H. K. SCHMID, *Proc. Electr. Micr. Soc. South. Afr.* **18** (1988) 35.
22. P. DOIG, D. LONSDALE and P. E. J. FLEWITT, *Phil. Mag.* **A41** (1980) 761.
23. E. K. W. GOO, R. K. MISHRA and G. THOMAS, *J. Amer. Ceram. Soc.* **64** (1981) 517.
24. L. PARDO, J. I. PINA and J. L. SACEDON, *J. Mater. Sci.* **23** (1988) 359.

Received 4 January
and accepted 23 August 1989